CrossMark

Experimental study on the diffusion–kinetics interaction in heterogeneous reaction of coal

Zeyang Song[1] · Xinyan Huang[2] · Minggang Luo[3] · Junhui Gong[1] · Xuhai Pan[1]

Abstract The diffusion of oxygen (O_2) plays an important role in the heterogeneous oxidation of coal and biomass, but is inadequately understood. This work aims to study the influence of intra-, inter-particle and external O_2 diffusions on the high-temperature heterogeneous oxidation using the TG-FTIR technique and two bituminous coals as example. Results show that coal sample of higher reactivity and smaller pore surface area is more sensitive to the O_2 diffusion. Specifically, increasing the size of particle, the reduced intra-particle (Knudsen) diffusion can reduce the conversion rate by 10–50%. While increasing the size of sample, the effective inter-particle diffusion shows a linear decrease. Comparatively, the influences of inter-particle and external diffusion in the TG scale (<5 mm) are weaker. For large TG samples (>10 mg) and low heating rates (2 K min^{-1}), the influence of thermal diffusion is strong enough to cause a thermal leap for the oxidation. Kinetic analysis using nth-order model-fitting method predicts the apparent activation energy (E) decreases with increasing reactivity. However, both model-free and Kissinger's methods show E increases with increasing reactivity,
against the physical definition of E. This work may help understand the diffusion–kinetics interaction in the fuel conversion and smoldering fire of coal and biomass.

Introduction

The diffusion of oxygen (O_2) plays an important role in heterogeneous reaction because it drives O_2 from the ambient into the surface of solid particles where chemical reaction takes place [1, 2]. For a typical heterogeneous reaction, three diffusive transport processes are involved: (1) external diffusion from the ambient to the external fuel surface, (2) inter-particle diffusion within the porous fuel bed and (3) intra-particle (pore) diffusion inside individual fuel particle. These diffusion processes can affect the chemical reaction, burning rate and pollutant emission. The interaction between surface chemical reaction and oxidizer diffusion can be categorized into three reaction regimes: kinetic control, reaction–diffusion control and diffusion control [3–6]. However, those regimes have not been quantitatively determined partly because of the complex interaction between heterogeneous reactions and O_2 transport.

In the literature, the diffusion of O_2, CO_2 and H_2O on the heterogeneous reaction of fossil fuels are mainly studied, e.g. low-temperature coal oxidation [4, 5, 7–9], char gasification/combustion [6, 10–15] and biomass smoldering [16, 17]. Low-temperature ($T < 500$ K) coal oxidation is responsible for the self-ignition and is an important fire safety issue [18]. Carpenter and Giddings [7] reported that the rate of O_2 consumption was limited by the rate of O_2

✉ Zeyang Song
  songzeyang03@126.com

  Xinyan Huang
  xinyan.huang@berkeley.edu

[1] Jiangsu Key Laboratory of Hazardous Chemicals Safety and Control, College of Safety Science and Engineering, Nanjing Tech University, Nanjing 211816, People's Republic of China

[2] Department of Mechanical Engineering, University of California, Berkeley, CA 94720, USA

[3] School of Energy Science and Engineering, Harbin Institute of Technology, Harbin 150001, People's Republic of China

diffusion within the coal pore. Krishnaswamy et al. [4] reported that in situ moisture significantly retarded the low-temperature coal oxidation as the moisture blocked the diffusion pathway. Wang et al. [5] concluded that the importance of diffusional and kinetic effects was associated with coal reactivity. Hull et al. [19, 20] modeled the role of O_2 diffusion in the ignition of a confined coal stockpile and showed that O_2 diffusion can lead to a maximum temperature rise of ~ 2150 K [6]. Zhang et al. [21] found for low-temperature coal oxidation in confined spaces, the O_2 consumption rate decreases with the size of coal particle. However, the retardance of O_2 diffusion for the fast oxidation at a higher temperature ($T > 800$ K) is still unknown, which may be more manifest and similar to high-temperature gasification process.

Driven by the clean coal technologies, diffusion in gasification become a hot research topic because of the development in char gasification. For example, Ollero et al. [14] proposed three standard sets of thermogravimetric (TG) experiments to assess the intrinsic gasification reactivity of char and the resistances of external and internal diffusions. Gómez-Barea et al. [10, 11] investigated the diffusion processes in the gasification of single biomass char particles in CO_2. Mani et al. [13] used the effective diffusivity, effectiveness factor and Thiele modulus to evaluate the diffusional effect on the gasification of biomass char in CO_2 and found diffusion was prominent at high temperature and for large particles. Similarly, Everson et al. [22] found the intraparticle diffusion controlled the rate of char combustion at high temperature. Gómez-Barea et al. [11] developed a simple methodology to assess fluid-dynamic and mass transport effects during kinetic experiments in a fluidized bed and established a 2-D non-isothermal and non-equimolar reaction–diffusion model to assess the diffusional effects on CO_2 gasification of a biomass char [23]. Diffusion in CO_2 gasification of torrefied and pyrolyzed flax straw chars [15], coke and coal char gasification with CO_2 [12] and steam [6] were studied in detail.

To meet environment-friendly demand, the techniques of fluidized bed combustion (FBC) [24–27], oxy-fuel combustion (OFC) [28–30] and underground coal gasification (UCG) [31–33] have been developed. Fundamentally, the chemical conversion of solid fuels into thermal energy or synthesis gas by the advanced techniques is the heterogeneous reaction, in which oxidizer diffusion could be expected to affect the conversion rate and kinetics. However, the literature review above indicates that very few studies have examined such hypothesis or the detailed role of O_2 diffusion in high-temperature heterogeneous oxidation. This paper aims to investigate the effects of intra-, inter-particle and external O_2 diffusions on high-temperature heterogeneous oxidation in TG scale and using coal as an example.

Experimental

Coal samples

Two bituminous coal samples were collected from Changchun (CC) and Xin'an (XA) Coal Mines in Henan Province, China. Fresh coal samples were maintained in well-sealed stainless steel cylindrical containers to prevent weathering. Coal samples were pulverized into five diameters (<74, 86.5, 111, 160.5 and 550 μm). Proximate and ultimate analyses of both bituminous coal samples are presented in Table 1. Also, the surface areas and average pore size shown in Fig. 1a were measured by the Autosorb-1 analyzer (Quantachrome Instruments), showing that pore surface area of CC coal sample is smaller than that of XA coal sample. The TESNSOR27 FTIR (Fourier Transform Infrared Spectroscopy) spectrometer (Bruker Optics, German) was used to examine the functional groups and the reactivity of raw coal samples, as presented in Fig. 1b.

TG-FTIR experiments

TG-FTIR experiments are the most widely used technique to study solid-phase kinetics as it provides a relatively well-controlled heating environment. In this work, STA449-F3 apparatus (NETZSCH, accuracy of 10^{-7} g) coupled with TESNSOR27 spectrometer (Bruker Optics, German) was used for non-isothermal TG tests. The coal sample was first dried by heating from 303 to 378 K in a nitrogen flow (100 mL min^{-1}) at the rate of 10 K min^{-1}, and after kept isothermal for 30 min, it was cooled back to 303 K. Subsequently, N_2 (80 mL min^{-1}) and O_2 (20 mL min^{-1}) were simultaneously purged into the furnace, and the sample temperature was elevated from 303 to 1173 K at three heating rates 2, 5 or 10 K min^{-1}. The

Table 1 Properties of studied coal samples

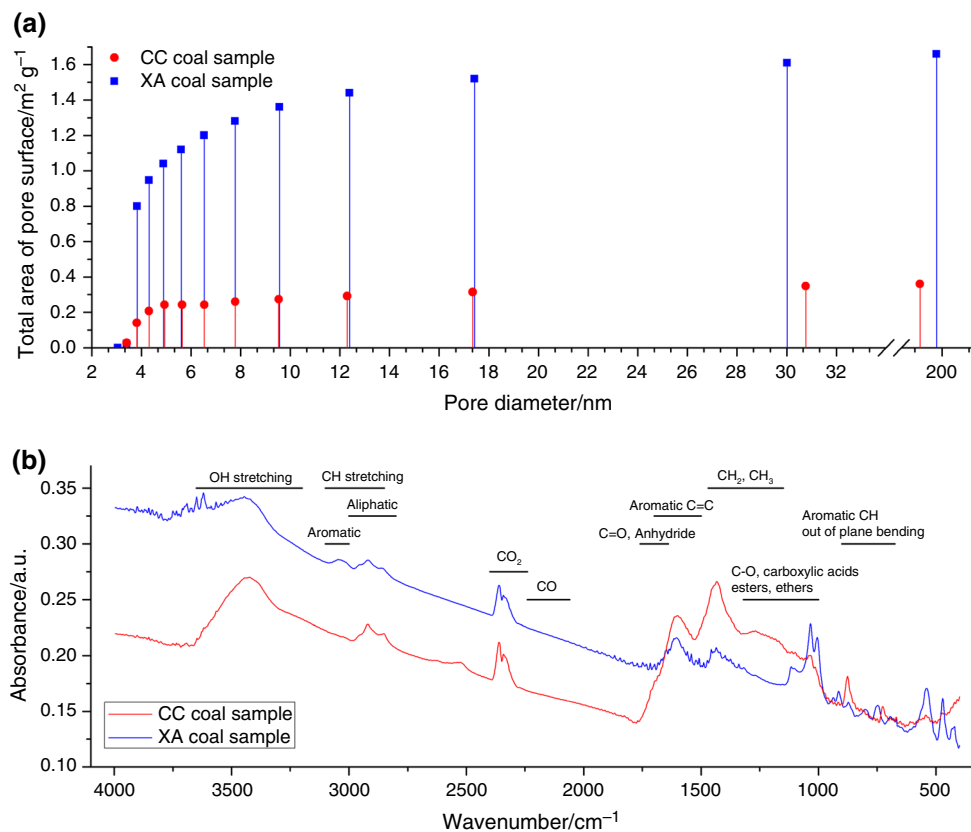| Basic properties		Changcun (CC)	Xin'an (XA)
Proximate analysis/%, Air-dried basis	Moisture	2.860	1.740
	Volatile	34.750	12.330
	Ash	14.840	14.120
	Fixed carbon	47.550	71.810
Ultimate analysis/%, Dry ash-free basis	Carbon	71.104	88.077
	Hydrogen	5.438	4.752
	Oxygen	21.880	3.990
	Nitrogen	1.313	1.680
	Sulfur	0.265	1.501
Pore surface area/m^2 g^{-1}		0.289	1.118
Average pore size/nm		1.780	1.727

Fig. 1 Coal properties of CC and XA coal samples: **a** pore surface distributions and **b** FTIR spectra of raw coal samples

volatile products and purging gasses were directly introduced into IR gas cell. The wavelength of FTIR spectrometry ranged from 650 to 4500 cm^{-1} where the spectral resolution was 4 cm^{-1}.

For heterogeneous reactions in TG test, there are three diffusive transport processes of O_2 [14]:

a. *Intra-particle (pore) diffusion* into the interior of fuel particles.
b. *Inter-particle diffusion* within the porous fuel bed.
c. *External diffusion* from the bulk ambient to the external layer of fuel bed.

Three test groups were designed to separate these diffusive processes (see Fig. 2; Table 2):

Group I (Intra-particle diffusion): Coal particles were homogeneously put on a circular aluminum oxide plate as a monolayer bed. For a monolayer, the difference only exists in the intra-particle diffusion. Five particle sizes (<74, 86.5, 111, 162.5 and 550 μm) were tested (I_1–I_5).

Group II (Inter-particle diffusion): Coal samples with the finest particle size (<74 μm, excluding the intra-particle diffusion) were fitted into an aluminum oxide cylindrical crucible until it was full (eliminating the external diffusion). Three diffusion lengths (2.7, 3.2 and 4.2 mm) were tested (II_1–II_3).

Group III (External diffusion): Coal samples with the finest particle size (<74 μm) were partially fitted into the crucible with external diffusional lengths of 1.5 and 1.0 mm (III_1 and III_2). Their inter-particle diffusional lengths were 2.7 and 3.2 mm, same as II_1 and II_2 in Group II.

For Group I, sample mass is smaller than 5 mg, below which the thermal and molecular diffusion effects are usually neglected. For large samples in Group II and III (>30 mg), diffusion and the self-heating should have a stronger influence on the mass loss rate. Calibration of heating rates and flow rates was carried out prior to TG experiments. Each scenario was carried out at least twice to check the repeatability, and the TG data difference was found to be less than 3%. The mass difference between repeated tests was less than ±4% for Group I and ±3% for Groups II and III.

Experimental

TG-FTIR analysis

Figure 3 shows the normalized mass loss rates (MLR, $\dot{m}$) of TG test at a heating rate of 5 K min^{-1}. In this work, Test I_1 (Group I) with the single-layer finest particle (<74 μm) has the minimum molecular and thermal diffusion effect.
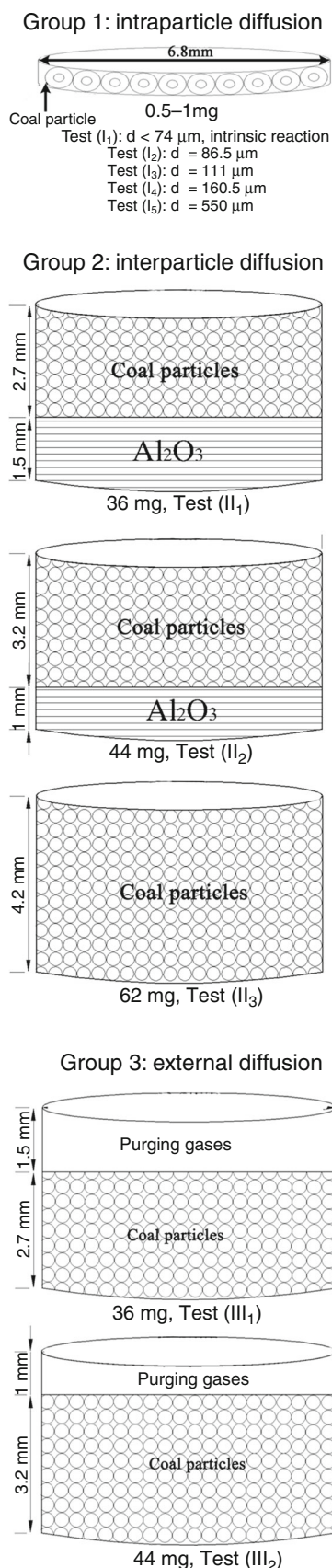
Group 1: intraparticle diffusion

6.8mm

Coal particle   0.5–1mg
Test (I_1): d < 74 μm, intrinsic reaction
Test (I_2): d = 86.5 μm
Test (I_3): d = 111 μm
Test (I_4): d = 160.5 μm
Test (I_5): d = 550 μm

Group 2: interparticle diffusion

2.7 mm   Coal particles
1.5 mm Al_2O_3
36 mg, Test (II_1)

3.2 mm   Coal particles
1 mm Al_2O_3
44 mg, Test (II_2)

4.2 mm   Coal particles
62 mg, Test (II_3)

Group 3: external diffusion

1.5 mm   Purging gases
2.7 mm   Coal particles
36 mg, Test (III_1)

1 mm   Purging gases
3.2 mm   Coal particles
44 mg, Test (III_2)

◀ **Fig. 2** Schematic diagrams of three experimental groups. Group I includes five subgroup tests (I_1–I_5) with five different particle sizes for intra-particle diffusion. Group II includes three tests (II_1–II_3) for inter-particle diffusion. Group III includes two tests (III_1 and III_2) for external diffusion

Therefore, Test I_1 is considered as the intrinsic reaction. In general, CC coal reaches the maximum oxidation at a lower temperature, showing a higher reactivity with O_2 than XA coal. Its ease for heterogeneous oxidation may arise from the fact that CC coal contains higher concentrations of function groups of C=O, aromatic C=C, anhydride and C–O (see Fig. 1b).

Figure 4 further presents the temperature evolution of CO_2 (characteristic bands at 2356/669 cm^{-1}), CO (2183/2119 cm^{-1}), methane (3018/1307 cm^{-1}) and SO_2 (1374 cm^{-1}) measured by FTIR spectra of Test II_1 for two coal samples. For the emission of CO_2, CO and CH_4, only one major peak between 500 and 900 K is found, and their peak locations overlap and agree with those of MLR curves shown in Fig. 3. However, for the SO_2 emission, two and three major peaks are found for CC and XA coal, respectively, indicating a complex multi-step decomposition process. For all test groups, the overall ratios of CO/CO_2 and $CH_4/(CO_2 + CO + CH_4)$ are 4.2 ± 0.3 and $0.4 \pm 0.1\%$ for CC coal, and 7.2 ± 0.4 and 0.4 ± 0.1% for XA coal, respectively. Thus, the CH_4 emission is similar for both coals, but more CO is produced in XA coal. Compared to the smoldering of coal ($CO/CO_2 > 10\%$ and $CH_4/(CO_2 + CO + CH_4) > 4\%$) [18], the current emission of CO and CH_4 is much smaller because of a good overall oxygen supply in the mg-scale TG experiment.

Diffusion effect analysis

For thermal analysis, the measured mass evolution is a function of temperature, which is usually evaluated by the conversion degree (α) [34].

$$\alpha(T) = \frac{m_0 - m(T)}{m_0 - m_\infty} \tag{1}$$

where m_0, m and m_∞ denote the mass of initial, current and final states, respectively. Qualitatively, for both coal samples, a smaller coal particle and a shorter diffusion length should lead to a faster reaction. The apparent reaction rate (r) is defined as the conversion rate [10, 14]:

$$r = \frac{d\alpha}{dt} \propto \dot{m} \tag{2}$$

which is proportional to MLR shown in Fig. 3 and has the same unit of s^{-1}.

Table 2 The configurations of diffusional TG experiments

TG tests		Sample mass/mg	Particle size d/μm	Sample thickness, l_{inter}/mm	External lengths, l_{exter}/mm
Group I (intra-particle diffusion)	I_1	0.45–0.5	74.0	–	–
	I_2	0.9–1.0	86.5	–	–
	I_3	1.3–1.34	111.0	–	–
	I_4	1.8–1.9	160.5	–	–
	I_5	2.4–2.5	550.0	–	–
Group II (inter-particle diffusion)	II_1	35.6–36.5	74.0	2.7	–
	II_2	43.8–44.2		3.2	–
	II_3	60.0–62.0		4.2	–
Group III (external diffusion)	III_1	36.0–38.0	74.0	2.7	1.5

To further quantify the changes in reaction rate by different diffusion processes, the effectiveness factor η is employed [4, 6, 35]. The *conversion effective factor* (η_c) is defined by the ratio of the global conversion of the apparent reaction (α_{app}) to that of the intrinsic reaction (α_{int}) in Test I_1 [10, 15, 35].

$$\eta_c(t) = \frac{\alpha_{app}(t)}{\alpha_{int}(t)} \tag{3}$$

which is a function of time. Its value at $\alpha_{int} = 50\%$ ($\eta_{c,50\%}$) is used as the representative to compare all single-layer samples in Group I, shown in Fig. 5.

To better compare between Group II and III, an alternative *reaction effective factor* (η_r) is defined by the ratio of the apparent reaction rate ($r_{app}(\alpha)$) to the intrinsic reaction rate ($r_{int}(\alpha)$) [6, 12, 14].

$$\eta_r = \frac{r_{app}(\alpha)}{r_{int}(\alpha)} \tag{4}$$

which is a function of the conversion degree (α). The value of η_r is often calculated using the average reaction rate ($\bar{r}$) from $\alpha = 1$ to 90% [36], shown in Fig. 6.

Intra-particle diffusional effects

As previously shown in Fig. 1a that for both CC and XA coal particles, most of the pores are tiny (less than 32 nm and accounting for ∼90% of total pore surface areas),
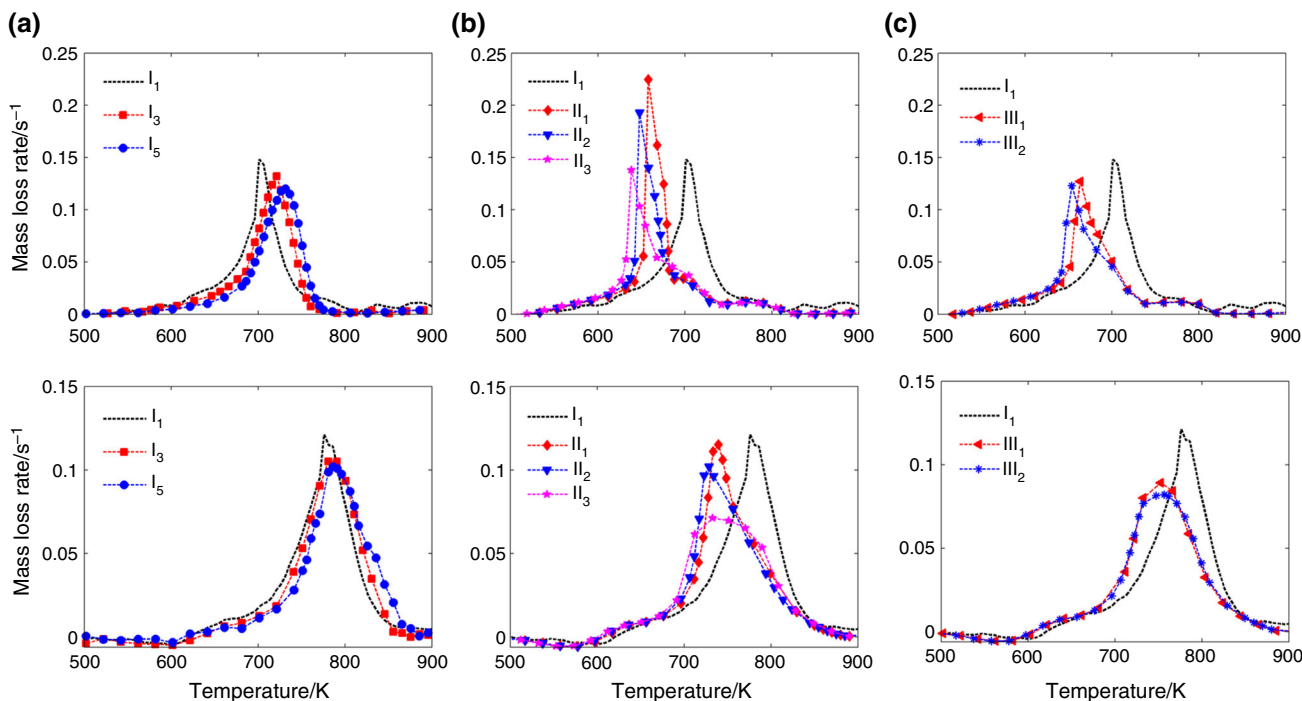

Fig. 3 Normalized mass loss rate ($\dot{m}$) curves of TG experiments at a heating rate of 5 K min^{-1}. **a** Intra-particle (pore) diffusion, **b** inter-particle diffusion and **c** external diffusion for CC (*upper*) and XA (*lower*) coal samples
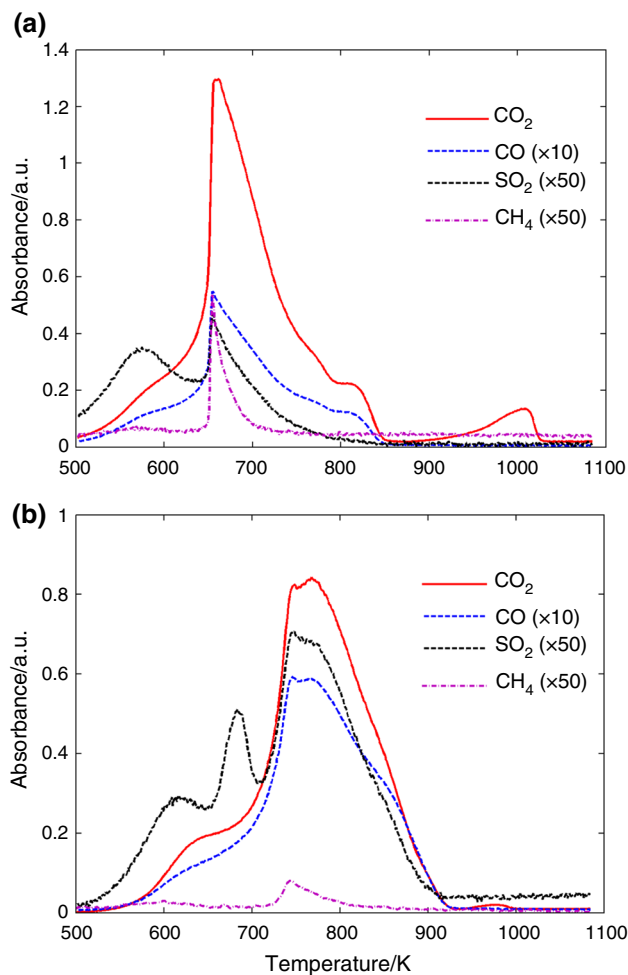
(a)

(b)

Fig. 4 Absorbance/temperature profiles of four gaseous emissions (CO_2, CO, SO_2 and CH_4) of Tests II_1 at 10 K min^{-1} heating rate for (**a**) CC and (**b**) XA coal samples
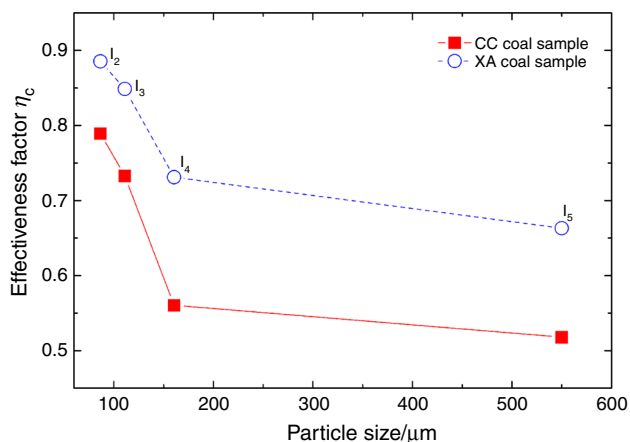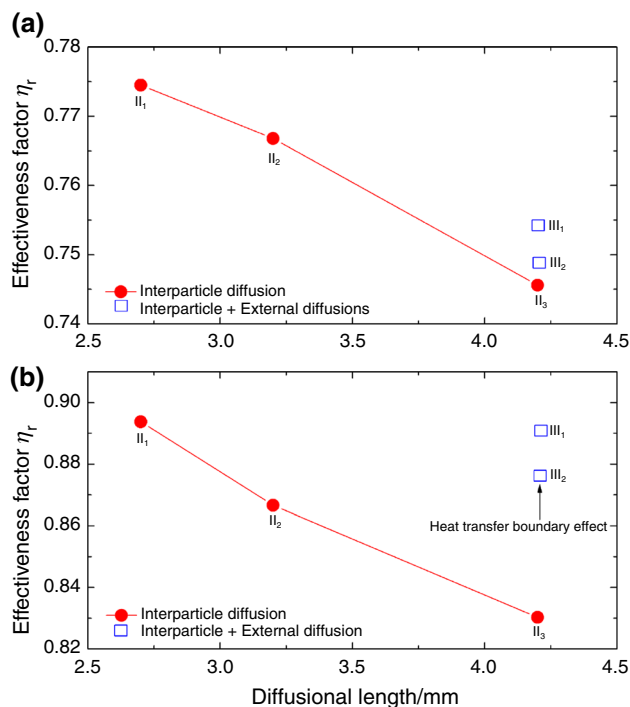

(a)

(b)

Fig. 6 Overall reaction effectiveness factors (η_r) of Groups II and III for **a** CC and **b** XA coal samples at the TG heating rate of 5 K min^{-1}

Fig. 5 Conversion effectiveness factor (η_c) versus particle size for CC and XA coal samples (Group I) at the TG heating rate of 5 K min^{-1}

and a small portion of large pores concentrates on a diameter of ~ 200 nm. It indicates that the Knudsen diffusion plays a dominant role in intra-particle diffusion [5, 6]. Figure 5 first shows that the effectiveness factor for CC coal sample is smaller compared to XA coal sample (similar results also found in Fig. 6), that is, CC coal is more sensitive to the O_2 diffusion. One possible reason is that the pore surface area of CC coal is smaller than that of XA coal (see Fig. 1a).

Figure 5 also shows that $\eta_{c,50\%}$ decreases with the increase in particle size for both coal samples, similar to the observation in char gasification [10, 15]. It indicates the O_2 intra-particle diffusion becomes relatively weak as the particle size increases. For example, the apparent reaction rate of 550 μm CC coal particles drops to $\sim 40\%$ of the conversion of the intrinsic reaction (74 μm particles). Moreover, such decreasing trend becomes very weak as the particle size increases above 200 μm, which is consistent with past results of low-temperature coal oxidation [4, 5] and gasification of char particles in CO_2 [10, 15].

Note that in previous studies, the low-temperature coal oxidation was independent of particle size [3, 5, 37], especially for fine particles (50–100 μm) [7]. However, such conclusion cannot be extended to high-temperature heterogeneous coal combustion. As indicated in Fig. 5, for the size of fine particle increasing from 74 to 111 μm, the combustion rate can significantly decrease, probably

because the oxidation rate increases exponentially with temperature. However, further increasing the size of particle, the oxidation rate eventually becomes limited by O_2 supply through the Knudsen diffusion.

Inter-particle diffusional effects

Figure 6 first shows that the inter-particle diffusion (red line) exerts an important influence on the rate of coal combustion. For example, for Test II_3 of CC coal sample, its reaction effective factor ($\eta_{r,II} = \eta_{r,in}$) is found to be 0.745. That is, compared to the intrinsic case (Test I_1), the inter-particle diffusion within 4.2 mm reduces the apparent reaction rate by 25.5%. Moreover, it is the first time that a linear relationship between $\eta_{r,in}$ and the inter-particle diffusion length (<5 mm) is found for two coal samples.

External diffusional effects

For test Group III (see blue squares in Fig. 6), both inter-particle and external diffusions are involved. With the same inter-particle diffusion length, their apparent reaction rates can be expressed as

$$r_{III} = \eta_{r,III} r_I \approx \eta_{r,ex} r_{II} \approx \eta_{r,ex} \eta_{r,II} r_I \qquad (5)$$

where subscripts "I–III" and "ex" represent the Group I–III and external diffusion, respectively. Therefore, we propose the reaction effective factor for external diffusion as

$$\eta_{r,ex} \approx \frac{\eta_{r,III}}{\eta_{r,II}} \qquad (6)$$

The values of $\eta_{r,ex}$ for test Group III are shown in Table 3. The retarding effect of the external diffusion increases with the rise of external diffusion length. Note that $\eta_{r,ex}$ for XA coal sample can be overestimated probably due to the influence of thermal boundary (discussed in Section 4.2).

Figure 6 also shows that despite the same overall diffusion length of 4.2 mm, the effectiveness factor of the Test II_3 (Group II) is smaller than that of Tests III_1 and Test III_2 (Group III). In other words, the resistance of inter-particle diffusion in porous fuel bed is more significant than the gas-phase external diffusion. Also, within the TG

Table 3 Reaction effectiveness factor of external diffusion ($\eta_{r,ex}$) lengths of 1 and 1.5 mm for CC and XA coal samples

Coal samples	$\eta_{r,ex}(l_{ex} = 1$ mm$)$	$\eta_{r,ex}(l_{ex} = 1.5$ mm$)$
CC	0.976	0.973
XA	1.011	0.996

length scale (<5 mm), both the inter-particle and external diffusions can only change the effectiveness factor within 0.1, much weaker than intra-particle diffusion. However, their influence is expected to increase with both increasing sample thickness and the distance between sample and free surface.

Discussions

Apparent activation energy

The concept of (apparent) activation energy (E) comes from the gas-phase reactions, and in general, it quantifies the difficulty of reaction occurrence. That is, a larger activation energy indicates a low reactivity. Obtaining activation energy is crucial for both kinetic analysis and numerical simulation. Recently, the concept of activation energy becomes widely used in solid-phase and heterogeneous reactions [13, 15, 29, 34, 38]. Here, the activation energy is also proposed to examine the reactivity of heterogeneous combustion of coal. To get the activation energy, there are two common approaches for the kinetic analysis: the model-free and model-fitting methods.

The model-free isoconversional (Friedman) method [39] is able to obtain the evolution of activation energy, and the conversion rate can be expressed as

$$\ln\left(\frac{d\alpha}{dt}\right)_{\alpha,i} = \ln(f(\alpha)A_\alpha) - \frac{E_\alpha}{RT_{\alpha,i}} \qquad (7)$$

where i denotes tests of variable heating rate, and A and E are the pre-exponential factor and activation energy, respectively. The value of E is a function of conversion degree (α), as summarized in Fig. 7. The reaction intervals, peak temperature and mass loss for kinetic calculation are represented in Table 4.

Figure 7 shows that E_α decreases as the reaction progresses for most TG experiments. More importantly, the obtained activation energy decreases with the decreasing O_2 supply via all three diffusion mechanisms (see Figs. 5, 6) or with decreasing overall oxidation rate (see Fig. 3). As shown in Table 4, peak temperature increases with increasing particle size. However, Fig. 8a further shows that the average activation energy decreases with increasing particle size. Note that these findings are completely in contradiction to the definition of activation energy, i.e., the activation energy increases as the reactivity decreases. Similar results were also found for other heterogeneous oxidation reactions including the oxidation of asphaltite [40], coal char [38], agricultural biomass [41], wood [42] and coal [8, 43] as well as the CO_2 gasification of char [15], different from non-oxidative pyrolysis reactions [44, 45].
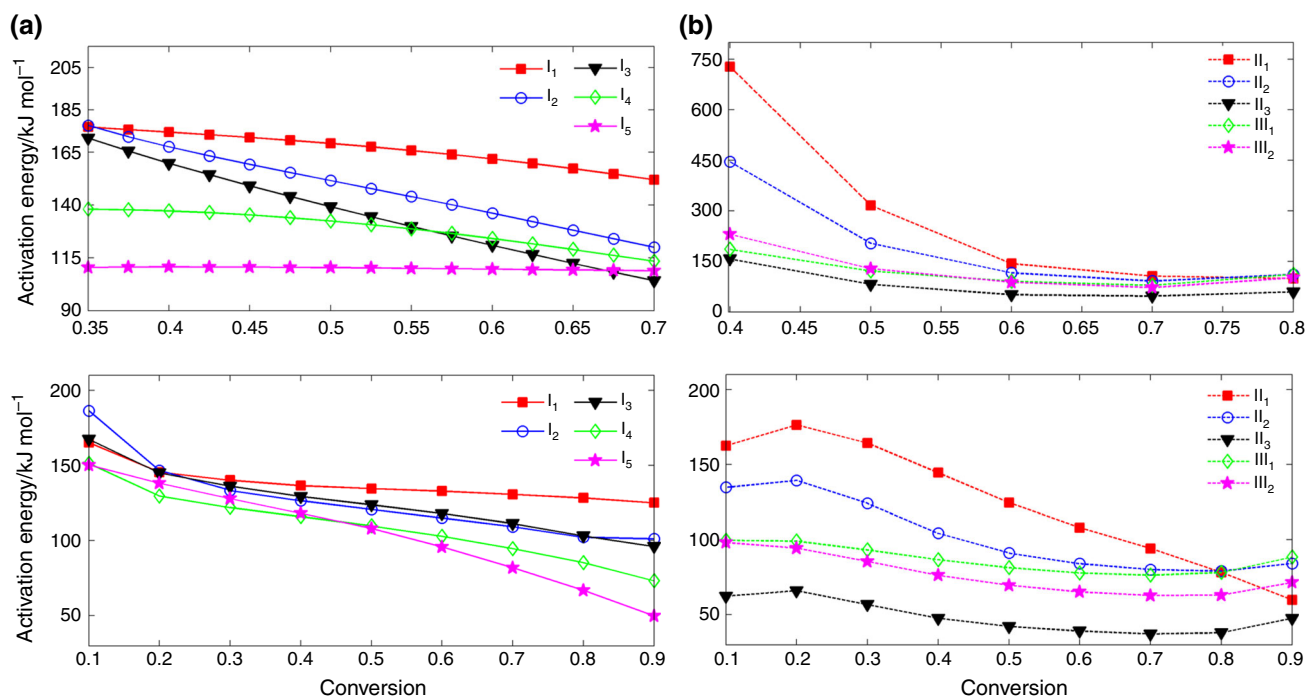
Fig. 7 Evolution of activation energy (E) with conversion (α): **a** intra-particle diffusion in Group I and **b** inter-particle and external diffusion in Groups II and III for CC (*upper*) and XA (*lower*) coal samples

Table 4 Reaction interval, peak temperature and mass loss of all TG tests at heating rate of 5 K min^{-1}

Test		Reaction interval/K		Peak temp./K		Mass loss/%	
		CC coal	XA coal	CC coal	XA coal	CC coal	XA coal
Group 1	I_1	691–726	706–815	716.1	785.9	41	82.9
	I_2	696–726	721–821	716.3	790.9	40	81.8
	I_3	701–731	726–826	721.4	791.0	41	81.6
	I_4	706–736	731–831	731.3	791.0	40	81.2
	I_5	711–741	736–841	736.4	791.1	41	82.0
Group 2	II_1	668–729	701–814	679.2	748.6	44.1	81.6
	II_2	665–723	696–809	647.9	738.6	40.0	81.2
	II_3	658–723	697–813	638.8	733.2	41.3	80.9
Group 3	III_1	671–733	701–814	676.6	757.1	45.3	81.3
	III_2	667–728	696–814	654.0	756.9	42.2	81.7

Therefore, it is inappropriate to use the obtained activation energy calculated by the model-free method to judge and compare the reactivity of heterogeneous oxidation of the same fuel.

Kissinger [46] proposed a simple analytical technique based on the temperatures of peak MLR under multiple heating rates. Note that the limitations of Kissinger's method include: (a) It does not include the whole information of TG data, but only a single point (i.e., the temperature at the peak MLR), and (b) the compensation effect between A and E is ignored [47]. Figure 8b shows the activation energy found by Kissinger's method. Compared to the model-free method in Fig. 8a, its value decreases with the increasing particle size or with the decreasing reaction rate. This trend is the same as the model-free method, against the definition of activation energy.

Besides the model-free and Kissinger's methods, the nth-order model-fitting method [46] can also be used to explain the TG data. Due to complicated chemical composition and physical structure, no universal reaction scheme can explain coal combustion. However, several general chemical reactions such as pyrolysis, gasification, coal oxidation and char oxidation have been acknowledged. Under certain conditions, coal combustion is dominated by the one-step reaction, and other reaction rate is slow and could be neglected. For instance, the low-volatile bituminous coal samples tested in this paper have a high carbon content, so the one-step overall char oxidation is dominant to result in a single MLR peak shown in Fig. 3.

Thus, we assume that combustion of two coal samples has a one-step global heterogeneous reaction (Coal + O_2 → CO_2 + CO + Ash). Then, the rate of heterogeneous reaction in Eq. (3) can be expressed by the Arrhenius law as follows
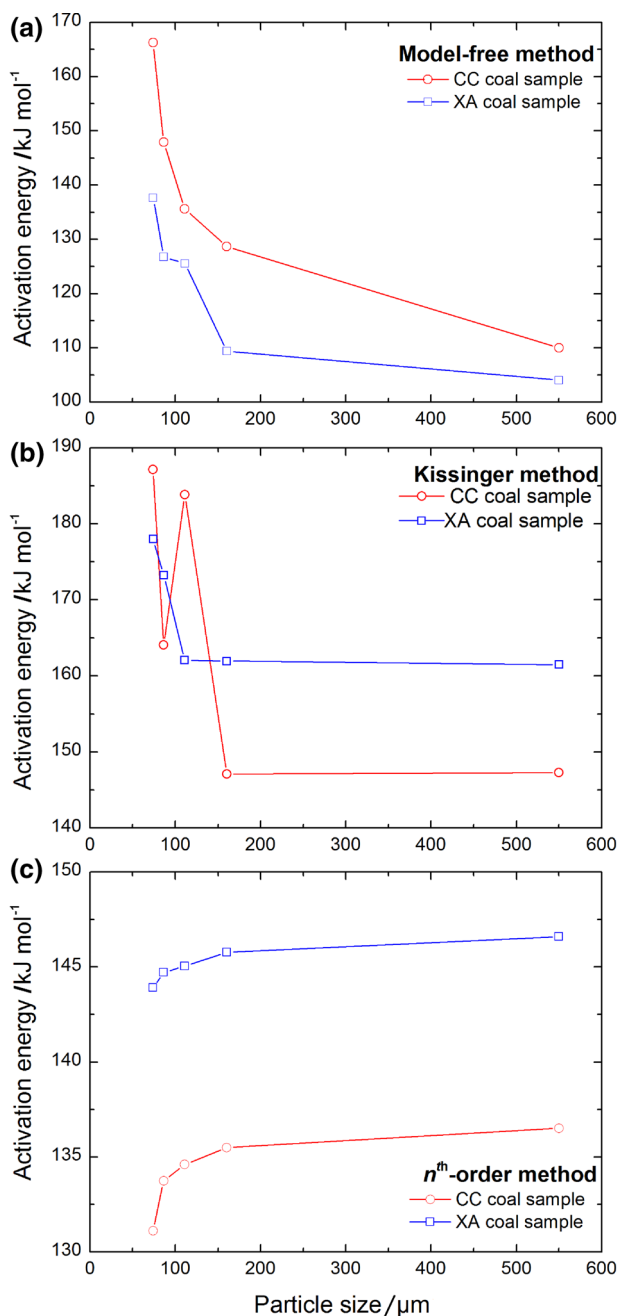
Fig. 8 Effect of particle size on the apparent activation energy evaluated by **a** model-free method, **b** Kissinger method and **c** *n*th-order method ($A = 1.26 \times 10^7$ and 8.00×10^6 for CC and XA coal samples, respectively)

$$r = Ae^{-\frac{E}{RT}}m^n \tag{8}$$

where *n* is the reaction order. One advantage of the *n*th-order model-fitting method is that there is only one unique value of activation energy (*E*) as well as *A* and *n* for each reaction if the TG data are sufficient [17]. Then, such unique activation energy can quantify its overall reactivity.
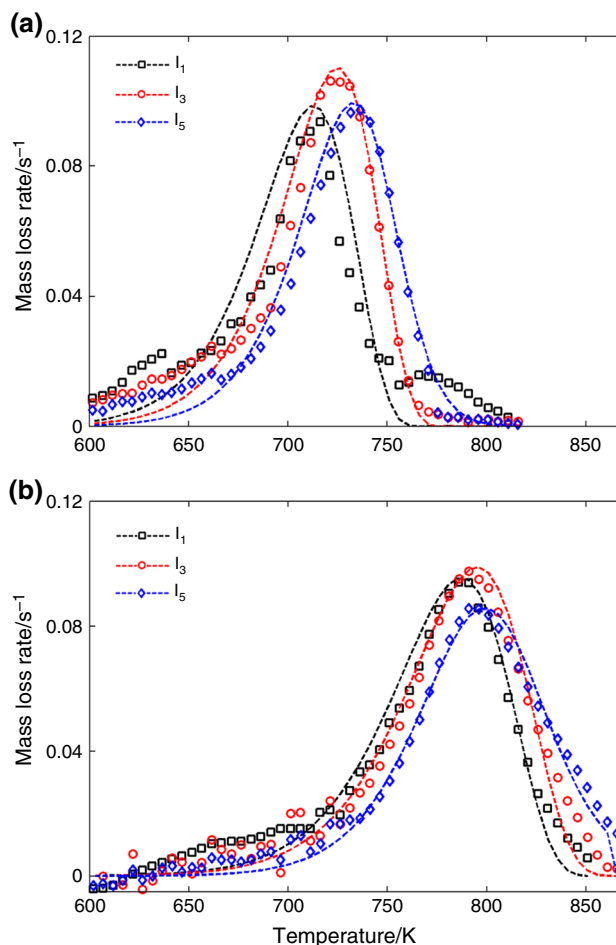

Fig. 9 Normalized mass loss rate (MLR) in TG (Group I) for **a** CC and **b** XA coal samples. *Dots* experiment. *Lines* simulation with kinetic parameters optimized by GA with a fixed pre-exponential factor

To accurately predict the TG data, a genetic algorithm (GA) is employed to search the best value of *A*, *E* and *n* (the kinetic triplet) for Eq. (8). GA is a stochastic global search method applying the principles of survival of the fittest of Darwinian evolution theory. Here, the optimization through GA aims to minimize the error between experimental and calculated MLR curves; see more details in the literature [17, 47]. To further avoid the compensation between *A* and *E*, the value of *A* is fixed for all particle sizes.

Figure 9 shows the simulated MLR curves using the kinetic parameters optimized by GA, which agrees well with experiments. The best solutions for apparent activation energy are shown in Fig. 9c with fixed $A = 1.26 \times 10^7$ and 8.00×10^6 s^{-1} for CC and XA coal samples, respectively. It is apparent that the obtained activation energy increases with the increasing particle size or with the decreasing reaction rate. This observation (a) agrees with the definition of activation energy and

(b) opposes to the results from the model-free method and Kissinger's method. Therefore, to use apparent activation energy to compare reactivity in oxidation, it is suggested to couple nth-order model-fitting method with GA and fix the value of pre-exponential factor.

Influence of heating rate and thermal diffusion

Ertunc and Kok [48], Kok [49] and Altun et al. [50] investigated effects of heating rate on heat flow, calorific value and kinetics of coal combustion. Reaction rate and peak temperature increase with the increase in heating rate [48, 49]. Relative slow heating rates (2, 5 and 10 K min^{-1}) were adopted in this study to slow rate of oxidation rate and to emphasize the interaction between oxygen diffusion and oxidation reaction in the TG domain. The heterogeneous coal combustion at high temperature is an exothermal process. For a single-layer coal sample (Group I), its heat release becomes negligible under the fast heat transfer between environment and sample. However, when the sample mass is over 10 mg (Groups II and III), the self-heating and temperature gradient within the sample can no longer be ignored. Such thermal diffusion effect may also

bring some biases to both the apparent reaction rate (the effectiveness factor) and the activation energy.

Figure 10 shows the MLR curves under different heating rates for Test I$_5$ and Test II$_3$ of CC coal sample. Figure 10a shows that the shape of MLR curve for the small sample in Test I$_5$ (<5 mg, see Table 2) is consistent with different heating rates, implying that same kinetic parameters can be used within the tested range of heating rates [46]. On the other hand, Fig. 10b shows that the curve shape changes greatly when sample masses are greater than 36 mg, and such change cannot be explained by the Arrhenius law. Also, at the slowest heating rate of 2 K min^{-1}, the peak decomposition rate of the large sample in Test II$_3$ is even higher than that of the smallest sample in Test I$_1$ (see Fig. 10b), resulting in $\eta_r > 1$. It may be because the thermal energy released by coal oxidation tends to increase the temperature of coal sample for Test II$_3$ with a large sample much faster than the slowest heating rate of 2 K min^{-1}. In that case, the sample temperature becomes higher than the environmental temperature,
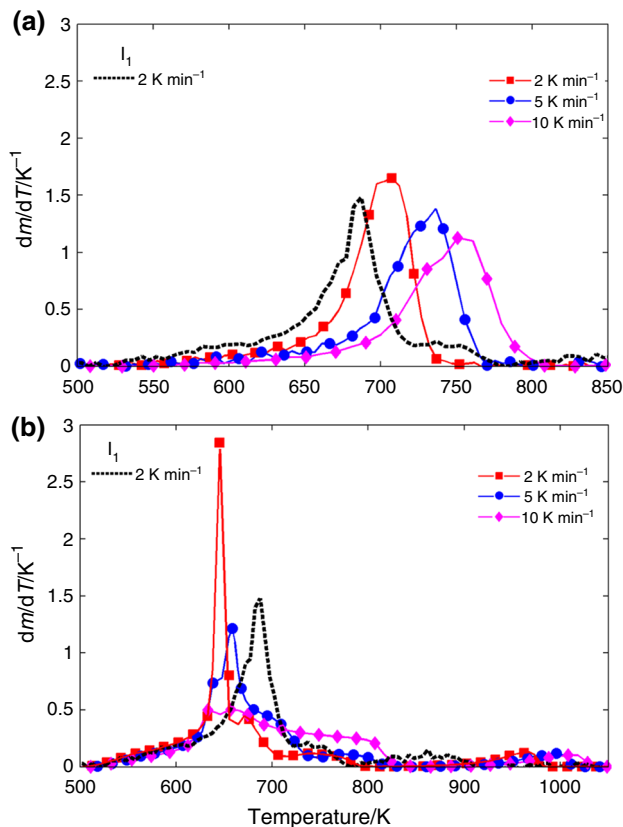

Fig. 10 Evolution of dm/dT with temperature in **a** Test I$_5$ and **b** Test II$_3$ for CC coal sample
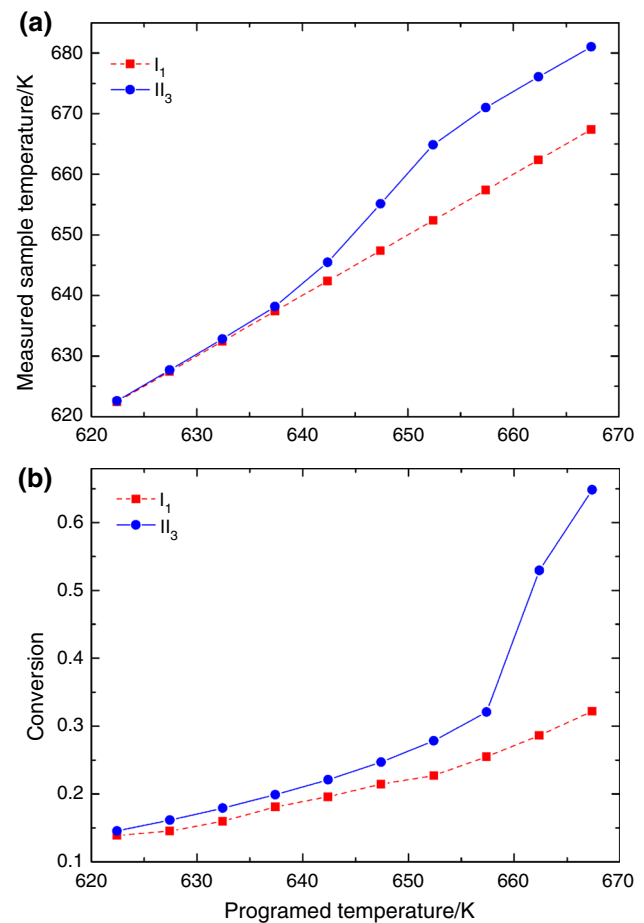

Fig. 11 Comparisons of **a** measured sample temperature and **b** conversion degree versus programmed temperature for small (Test I$_1$) and large (Test II$_3$) CC coal sample at a slow heating rate of 2 K min^{-1}

Table 5 Comparison of effectiveness factors of coal combustion and char gasification

Refs.	Solid fuel	Reactive gas	Temperature	Particle size	Methods	Effectiveness factors
[14]	Olive char	CO_2	Isothermal: 1073–1223 K	<150 μm	$\eta_{c,50\%}$	Internal: 0.25–0.50
						External: 0.63–1.00
[10]	Biomass char	CO_2	Isothermal: 1073–1223 K	0.06–2.1 mm	η_r	Intra-particle: 0.22–0.90
[13]	Wheat straw char	CO_2	Isothermal: 1023–1223 K	<60–925 μm	Equation (9)[a]	Internal: $\sim$0.70–0.95
[6, 12]	Coke and coal char	CO_2, H_2O	Isothermal: 1123–1573 K	<40–500 μm	η_r	Intra-particle: $\sim$0.20–1.00
This study	Bituminous coal	O_2	Non-isothermal: 303–1173 K	<74–500 μm	$\eta_{c,50\%}$ and η_r	Intra-particle: 0.50–0.80 (more reactive CC coal sample) and 0.70–0.90 (XA coal sample)
						Inter-particle: 0.74–0.90; External: >0.97 (diffusion length: 2.7–4.2 mm)

[a] Equation (9): $\eta = 1/\varphi \tanh 3\varphi - 1/3\varphi$, where φ is the Thiele modulus

leading to a "thermal leap" which is opposite to the "thermal lag" in the high heating rate.

Such hypothesis is demonstrated in Fig. 11 where under the programmed temperature of 620–670 K and the slow heating rate of 2 K min^{-1}, both the measured sample temperature and conversion degree in Test II$_3$ are higher than those in Test I$_1$. Therefore, the overall MLR at Test II$_3$ peaks at a lower programmed temperature than Test I$_1$ (see Fig. 10b). In other words, if the sample has a large mass and involves heterogeneous oxidation, a small heating rate equal to or smaller than 2 K min^{-1} is not recommended in TG, because of the potential thermal leap in the result.

Besides the influence of small heating rate, the thermal boundary condition in TG cannot be ignored for large samples either. Comparing the sample configurations between Tests II$_2$ and III$_2$ in Fig. 2, Test II$_2$ has an additional Al$_2$O$_3$ base to avoid the external diffusion. However, the Al$_2$O$_3$ base also creates an additional thermal resistance between the sample and hot environment. Such thermal resistance may be responsible for the abnormal $\eta_{r,ex}(l_{ex} = 1$ mm$) > 1$ found in Fig. 6 and Table 2.

In short, for these large samples, neither the model-free nor the nth-order model-fitting method can effectively evaluate the activation energy because the thermal diffusion in the solid phase becomes very important. Interestingly, despite the uncertainty, the determined E_α for Groups II and III in Fig. 7b by the model-free method increases with increasing reactivity, similar to that for Group I in Fig. 7a. To further quantify both molecular and thermal diffusion processes and their interaction with heterogeneous reactions, a numerical approach may be necessary, and it will be conducted in future work.

Comparison of coal gasification and char gasification

The effectiveness factor (η) in past studies is summarized in Table 5, which varies in a wide range due to different experimental conditions, calculation methods and materials. The comparison shows that for both coal combustion and gasification [14], the influence of the external diffusion is the smallest in TG scale. Because O_2 is more reactive and has a high bimolecular diffusivity than CO_2 and coal is more active and less porous than char, it is expected that the retarding effect of O_2 diffusion on coal gasification should be more predominant than that of CO_2 diffusion on char gasification.

Conclusions

In this work, the influences of intra-, inter-particle and external O_2 diffusions on the heterogeneous oxidation are studied using TG-FTIR analysis of coal. Both conversion (η_c) and reaction (η_r) effectiveness factors successfully quantify the reduction in apparent reaction rates by different diffusion processes. The pore diffusion exhibits the strongest retarding influence on the heterogeneous reaction of coal. With the increasing particle size, the change in intra-particle diffusion can significantly lower the apparent reaction rate by 10–30% for the finer coal particles ($\leq$111 μm) and by $\sim$50% for coarser coal particles (>111 μm). The pore structure of coal indicates that the Knudsen diffusion mainly accounts for the pore diffusion. Comparatively, the apparent reaction rate is weakly

affected by either inter-particle or external diffusions in the TG domain (<5 mm). However, for a large TG sample (>10 mg), the thermal diffusion effect cannot be neglected, and using a slow TG heating rate (2 K min^{-1}) for oxidation can lead to a thermal leap.

The interaction between diffusion and activation energy is successfully explored by kinetic analysis using Kissinger's, model-free and model-fitting methods. The apparent activation energy, obtained from the nth-order model-fitting method, decreases with increasing reactivity. However, using model-free and Kissinger's methods, the obtained apparent activation energy increases with increasing reactivity, which is against the physical definition of activation energy. Thus, it is not suggested to use activation energy estimated by model-free and Kissinger's methods to estimate the influence of diffusion on heterogeneous oxidation or gasification. Moreover, because O_2 has the higher reactivity and bimolecular diffusivity, coal combustion or gasification is found to be more sensitive to the O_2 diffusion than the CO_2 diffusion in the char gasification. This work may help understand the interaction between O_2 transport and heterogeneous reaction in coal and biomass conversion techniques such as FBC, OFC and UGC. In addition, it may help explain the initiation and development of smoldering fires of underground coal seam and confined coal and biomass piles.

References

1. Brown NJ, Bastien LA, Price PN. Transport properties for combustion modeling. Prog Energ Combust. 2011;37:565–82.
2. Kumar A, Mazumder S. Assessment of various diffusion models for the prediction of heterogeneous combustion in monolith tubes. Comput Chem Eng. 2008;32:1482–93.
3. Wang H, Dlugogorski BZ, Kennedy EM. Coal oxidation at low temperatures: oxygen consumption, oxidation products, reaction mechanism and kinetic modelling. Prog Energ Combust. 2003;29:487–513.
4. Krishnaswamy S, Bhat S, Gunn RD. Low–temperature oxidation of coal 1. A single–particle reaction–diffusion model. Fuel. 1996;75:333–43.
5. Wang H, Dlugogorski B, Kennedy E. Theoretical analysis of reaction regimes in low–temperature oxidation of coal. Fuel. 1999;78:1073–81.
6. Huo W, Zhou Z, Wang F, Wang Y, Yu G. Experimental study of pore diffusion effect on char gasification with CO_2 and steam. Fuel. 2014;131:59–65.
7. Carpenter DL, Sergeant GD. The initial stages of the oxidation of coal with molecular oxygen. III. Effect of particle size on rate of oxygen consumption. Fuel. 1966;45:311–27.
8. Akgun F, Arisoy A. Effect of particle size on the spontaneous heating of a coal stockpile. Combust Flame. 1994;99:137–46.
9. Bouwman R, Freriks IL. Low-temperature oxidation of a bituminous coal. Infrared spectroscopic study of samples from a coal pile. Fuel. 1980;59:315–22.
10. Gómez-Barea A, Ollero P, Fernández-Baco C. Diffusional effects in CO_2 gasification experiments with single biomass char particles. 1. Experimental investigation. Energ Fuel. 2006;20: 2202–10.
11. Gómez-Barea A, Ollero P, Leckner B. Mass transport effects during measurements of gas–solid reaction kinetics in a fluidised bed. Chem Eng Sci. 2007;62:1477–93.
12. Huo W, Zhou Z, Wang F, Yu G. Mechanism analysis and experimental verification of pore diffusion on coke and coal char gasification with CO_2. Chem Eng Sci. 2014;244:227–33.
13. Mani T, Mahinpey N, Murugan P. Reaction kinetics and mass transfer studies of biomass char gasification with CO_2. Chem Eng Sci. 2011;66:36–41.
14. Ollero P, Serrera A, Arjona R, Alcantarilla S. Diffusional effects in TGA gasification experiments for kinetic determination. Fuel. 2002;81:1989–2000.
15. Vincent SS, Mahinpey N, Aqsha A. Mass transfer studies during CO_2 gasification of torrefied and pyrolyzed chars. Energy. 2014;67:319–27.
16. Huang X, Rein G. Thermochemical conversion of biomass in smouldering combustion across scales: the roles of heterogeneous kinetics, oxygen and transport phenomena. Biosource Technol. 2016;207:409–21.
17. Huang X, Rein G. Smouldering combustion of peat in wildfires: Inverse modelling of the drying and the thermal and oxidative decomposition kinetics. Combust Flame. 2014;161:1633–44.
18. Wu D, Schmidt M, Huang X, Verplaetsen F. Self-ignition and smouldering of coal dust accumulations in O_2/N_2 and O_2/CO_2 atmospheres. Proc Combust Inst. 2017;36:3195–202.
19. Hull A, Lanthier JL, Agarwal PK. The role of the diffusion of oxygen in the ignition of a coal stockpile in confined storage. Fuel. 1997;76:975–83.
20. Hull AS, Lanthier JL, Chen Z, Agarwal PK. The role of the diffusion of oxygen and radiation on the spontaneous combustibility of a coal pile in confined storage. Combust Flame. 1997;110:479–93.
21. Zhang Y, Wu J, Chang L, Wang J, Li Z. Changes in the reaction regime during low–temperature oxidation of coal in confined spaces. J Loss Prevent Proc. 2013;26:1221–9.
22. Everson RC, Neomagus HW, Kaitano R. The random pore model with intraparticle diffusion for the description of combustion of char particles derived from minera and inertinite rich coal. Fuel. 2011;90:2347–52.
23. Gómez-Barea A, Ollero P, Arjona R. Reaction–diffusion model of TGA gasification experiments for estimating diffusional effects. Fuel. 2005;84:1695–704.
24. Anthony EJ. Fluidized bed combustion of alternative solid fuels; status, successes and problems of the technology. Prog Energ Combust. 1995;21:239–68.
25. Liu B, Yang X, Song W, Lin W. Process simulation development of coal combustion in a circulating fluidized bed combustor based on aspen plus. Energ Fuel. 2011;25:1721–30.
26. Murakami T, Suzuki Y, Durrani AK. New Approach to understanding NO emission during bubbling fluidized bed coal combustion: separation of NO formation and reduction processes in the bed. Energy Fuel. 2010;23:1950–5.
27. Glazer MP, Khan NA, de Jong W, Spliethoff H, Schürmann H, Monkhouse P. Alkali metals in circulating fluidized bed combustion of biomass and coal: measurements and chemical equilibrium analysis. Energy Fuel. 2005;19:1889–97.

28. Belo LP, Spörl R, Shah KV, Elliott LK, Stanger RJ, Maier J, Wall TF. Sulfur capture by fly ash in air and oxy–fuel pulverized fuel combustion. Energ Fuel. 2014;28:5472–9.

29. Nunes KGP, Osório E, Marcílio NR. Kinetics of the oxy–fuel combustion of high-ash-content coal from the Candiota mine. Rio Grande do Sul. Energ Fuel. 2016;30:1958–64.

30. Buhre BJP, Elliott LK, Sheng CD, Gupta RP, Wall TF. Oxy-fuel combustion technology for coal-fired power generation. Prog Energ Combust. 2005;31:283–307.

31. Bhutto AW, Bazmi AA, Zahedi G. Underground coal gasification: From fundamentals to applications. Prog Energ Combust. 2013;39:189–214.

32. Peng P, Barse K, Nasah J. Competitiveness and cost sensitivity study of underground coal gasification combined cycle using lignite. Energ Fuel. 2016;30:2111–8.

33. And GP, Sahajwalla V. A Mathematical model for the chemical reaction of a semi-infinite block of coal in underground coal gasification. Energ Fuel. 2005;19:1679–92.

34. Vyazovkin S, Chrissafis K, Di Lorenzo ML, Koga N, Pijolat M, Roduit B, Sbirrazzuoli N, Suñol JJ. ICTAC Kinetics Committee recommendations for collecting experimental thermal analysis data for kinetic computations. Thermochim Acta. 2014;590:1–23.

35. Ramachandran P. Analytical prediction of conversion-time behaviour of gas-solid noncatalytic reactions. Chem Eng Sci. 1983;38:1385–90.

36. Vyazovkin S, Burnham AK, Criado JM, Pérez-Maqueda LA, Popescu C, Sbirrazzuoli N. ICTAC Kinetics Committee recommendations for performing kinetic computations on thermal analysis data. Thermochim Acta. 2011;520:1–19.

37. Carras JN, Young BC. Self-heating of coal and related materials: models, application and test methods. Prog Energ Combust. 1994;20:1–15.

38. Kim RG, Jeon CH. Intrinsic reaction kinetics of coal char combustion by direct measurement of ignition temperature. Appl Therm Eng. 2014;63:565–76.

39. Friedman HL. Kinetics of thermal degradation of char-forming plastics from thermogravimetry. Application to a phenolic plastic. J Polym Sci C. 1964;6:183–95.

40. Altun NE, Kok MV, Hicyilmaz C. Effect of particle size and heating rate on the combustion of silopi asphaltite. Energ Fuel. 2002;16:785–90.

41. Garciamaraver A, Perezjimenez JA, Serranobernardo F, Zamorano M. Determination and comparison of combustion kinetics parameters of agricultural biomass from olive trees. Renew Energ. 2015;83:897–904.

42. Shen DK, Gu S, Jin B, Fang MX. Thermal degradation mechanisms of wood under inert and oxidative environments using DAEM methods. Bioresour Technol. 2011;102:2047–52.

43. Wu D, Huang X, Norman F, Verplaetsen F, Berghmans J, Van den Bulck E. Experimental investigation on the self-ignition behaviour of coal dust accumulations in oxy-fuel combustion system. Fuel. 2015;160:245–54.

44. Kök MV, Özbas E, Karacan O, Hicyilmaz C. Effect of particle size on coal pyrolysis. J Anal Appl Pyrol. 1998;45:103–10.

45. Güldoğan Y, Durusoy T, Bozdemir T. Effects of heating rate and particle size on pyrolysis kinetics of gediz lignite. Energ Source. 2002;24:753–60.

46. Kissinger HE. Reaction kinetics in differential thermal analysis. Anal Chem. 1957;29:1702–6.

47. Li KY, Huang X, Fleischmann C, Rein G, Ji J. Pyrolysis of medium-density fiberboard: optimized search for kinetics scheme and parameters via a genetic algorithm driven by Kissinger's method. Energ Fuel. 2014;28:6130–9.

48. Ertunc G, Kok MV. Determination of kinetic parameters of different origin coals using software. J Therm Anal Calorim. 2015;119:1–7.

49. Kok MV. Simultaneous thermogravimetry–calorimetry study on the combustion of coal samples: effect of heating rate. Energ Convers Manage. 2012;53:40–4.

50. Altun NE, Hicyilmaz C, Kök MV. Effect of particle size and heating rate on the pyrolysis of Silopi asphaltite. J Anal Appl Pyrol. 2003;67:369–79.